

# Mass fractions in stellar interior during presupernova evolution

Jameel-Un Nabi<sup>1</sup> • Abdel Nasser Tawfik<sup>2</sup> •  
Nada Ezzelarab<sup>2</sup> • Ali Abas Khan<sup>1</sup>

**Abstract** We assume nuclear statistical equilibrium (NSE) conditions and use Saha Equation to calculate mass fractions in stellar interior during presupernova evolution of massive stars. Our ensemble contains 728 nuclei. The distinguishing feature of our calculation is a state-by-state summation of nuclear level densities up to 10 MeV for all nuclei considered in our ensemble. This leads to a more realistic description of nuclear partition function which poses one of the largest uncertainties in the mass fraction calculations under conditions of NSE. The Coulomb correction term was taken into account for the calculation of ground-state binding energies of the nucleons. Our calculated mass fractions are up to four orders of magnitude smaller than previous calculation. The current calculation could prove useful for study of stellar matter during presupernova phases of massive stars.

**Keywords** Nuclear Statistical Equilibrium, Nuclear Level Density, Nuclear Partition Function, Nuclear Abundance, Mass Fractions, Stellar Core-Collapse.

---

Jameel-Un Nabi

Faculty of Engineering Sciences, GIK Institute of Engineering Sciences and Technology, Topi 23640, Swabi, Khyber Pakhtunkhwa, Pakistan

Abdel Nasser Tawfik

Egyptian Center for Theoretical Physics, MTI Modern University, Al Mokattam, 11571 Cairo, Egypt

Nada Ezzelarab

Egyptian Center for Theoretical Physics, MTI Modern University, Al Mokattam, 11571 Cairo, Egypt

Ali Abas Khan

GIK Institute of Engineering Sciences and Technology, Topi 23640, Khyber Pakhtunkhwa, Pakistan

<sup>1</sup>Corresponding author email : jameel@giki.edu.pk

## 1 Introduction

The study of various models of the explosive nucleosynthesis as well as the  $r$ -process (Ptitsyn & Chechetkin 1982; Woosley & Hoffman 1992; Nadyozhin et al. 1998) requires knowledge of the chemical composition close to the nuclear statistical equilibrium (NSE), which is as an initial condition for nuclear reaction network calculations. In NSE scenario, an equilibrium is achieved between strong and electro-magnetic interactions for all sort of nuclear species. The weak interaction, however, is not in equilibrium as the stellar matter is transparent to neutrinos produced and energy is channeled out of the system. Under the assumption of NSE, the isotropic abundances of nuclei follow simply from nuclear Saha's equation for a given density, temperature, and electron fraction (Hartmann et al. 1985). Under NSE condition, each nucleus can be transformable to any other nucleus and the radiation and matter must be in equilibrium in the stellar assembly. Details of NSE conditions can be seen in (Hoyle 1954). During stellar evolution, when silicon burning terminates, all nuclear reactions are studied by the NSE. A number of authors studied the problem of NSE by using Saha's type equations (Hartmann et al. 1985; Men-Quan et al. 2007; Clifford & Tayler 1965; Epstein & Arnett 1975; Aufderheide et al. 1994; Bravo & García-Senz 1999).

The thermodynamic conditions spanned over several 100 ms time interval post bounce in core-collapse supernova simulation have been analyzed (Fischer et al. 2014), where the density range spanned about 10 orders of magnitude ( $10^5 - 10^{15} \text{ g cm}^{-3}$ ), the temperature around two orders (0.1 - 50 MeV) and the lepton fraction more than an order of magnitude (0.01 - 0.5). The large variety of nuclear matter properties leads to distinct outcomes in supernova simulations.

The rate of change of lepton-to-baryon fraction ( $Y_e$ ) depends both on mass fractions and weak-interaction rates of the nuclei. The acceleration of core-collapse of massive stars changes with NSE. Recently we studied the evolution of composition of nuclear matter over a wide temperature ( $10^9 - 10^{11}$  K) and density range ( $10^1 - 10^{11}$  g cm $^{-3}$ ) (Nabi et al. 2015). In the present paper we study the mass fractions of nuclei and free nucleons as a function of  $Y_e$  of the stellar matter. Our ensemble contained a total of 728 nuclei, having mass number up to 100 which were selected primarily to cover a decent number of nuclei for astrophysical simulations.

Accurate and reliable values of nuclear partition function (NPF) are a prerequisite for the determination of the mass fractions in the presupernova matter. NPF also plays key role in other astrophysical processes, e.g. determination of equation of state during gravitational collapse (Fuller 1982) and abundances isotopic calculations in silicon burning (Hix & Thielemann 1996). In a recent study of isotopic abundances in presupernova cores (Dimarco et al. 2002), it was concluded that low-lying nuclear states need to be treated preferably as discrete and a summation over these states lead to significant change in the calculated value of NPF which in turn poses one of the biggest uncertainty in the calculation of mass fractions. The calculated NPF by the authors showed a deviation of up to 50% when discrete energy levels were considered as against those assuming a level density function and performing integrals to obtain the NPF. However the authors in (Dimarco et al. 2002) were able to perform summation over discrete energy levels only up to 3 MeV. We performed summation for all discrete energy levels up to 10 MeV in our present calculation. The pn-QRPA model was used to calculate all discrete energy levels up to 10 MeV. Soaring stellar temperatures prior to collapse gives a finite contribution to NPF even up to 10 MeV. Beyond 10 MeV we do assume a level density function in our calculation of NPF. Further to this, authors in (Dimarco et al. 2002) used a total of 65 nuclear species in their calculation whereas the current paper deals with a much bigger ensemble of 728 nuclei.

The present paper is organized as follows. Section 2 briefly describes the formalism which we adopted to calculate mass fractions, nuclear level density and NPF. Section 3 discusses our results and also compares our calculation with previous calculation. We finally conclude our findings in Section 4.

## 2 Formalism

Our NSE treatment is similar to that employed by (Hartmann et al. 1985; Clifford & Tayler 1965;

Aufderheide et al. 1994; Kodama & Takahashi 1975). Under NSE the mass fraction for nuclei other than neutrons and protons is given by the Saha equation

$$X(A, Z) = \frac{G(A, Z, T)}{2} \left( \frac{\rho_{st} N_0 \lambda_T^3}{2} \right)^{A-1} \times A^{\frac{5}{2}} X_n^{A-Z} X_p^Z \exp[B(A, Z)/kT]. \quad (1)$$

where  $X_n$  and  $X_p$  are the mass fractions of free neutron and protons, respectively,  $G(A, Z, T)$  is the temperature-dependent nuclear partition function,  $B(A, Z)$  is the ground state binding energy,  $T$  is stellar temperature,  $\lambda_T$  is the thermal wavelength,  $k$  is the Boltzmann constant,  $A$  is the mass number,  $\rho_{st}$  is the stellar density and  $N_0$  is Avogadro's number. Neglecting the Coulomb's correction, the ground state binding energy  $B(A, Z)$  is given by

$$B(A, Z) = c^2 [Nm_n + Zm_p - m(A, Z)], \quad (2)$$

where  $m_n$ ,  $m_p$  and  $m(A, Z)$  denote the masses of free neutrons, protons and nuclei, respectively. Due to electron screening the nuclear binding energies in stellar environment should be different than those in the vacuum (?). Consequently, driplines are shifted and the heavy nuclei become unstable against fission under terrestrial condition. However they may become stable in supernova matter. These might be very important under astrophysical conditions. We included the Coulomb's correction in binding energy equation using Hartree-Fock approximation in Wigner-Seitz cells (Chamel et al. 2007). When Coulomb's correction is take into account the ground state binding energy gets the form

$$B(A, Z)^{cc} = B(A, Z) - \Delta V_f^{cc}(\rho_e), \quad (3)$$

where

$$\Delta V_f^{cc}(\rho_e) = -\frac{3}{5} \frac{Z^2 e^2}{R_0} \left( \frac{3}{2} \eta - \frac{1}{2} \eta^3 \right), \quad (4)$$

here  $\eta = \frac{n_e}{n_0} \frac{A}{Z}$  and  $n_e$  represents free electron density. We assume nucleons as a homogeneous sphere of radius  $R_0$  at a maximum density  $n_0$ . Radius of the sphere is given by

$$R_0 = \left( \frac{3A}{4\pi n_0} \right)^{1/3}. \quad (5)$$

Temperature dependent NPF plays a key role in calculation of abundance of nuclear species. An improvement was made in this study to use a true temperature dependent NPF,  $G(A, Z, T)$ , compared to previous calculations of NPF e.g. (Epstein & Arnett 1975). The

NPF over discrete energy levels can be calculated using

$$G(A, Z, T) = \sum_i (2J_i + 1) \exp[-E_i/kT], \quad (6)$$

here  $J_i$  and  $E_i$  denotes spin and energy of the  $i^{\text{th}}$  state. However it is a well-known fact that the discrete energy levels become continuous as the excitation energy increases and then a more generalized nuclear partition function with level densities normalized to ground state energy is given by (Fowler et al. 1967):

$$G(A, Z, T) = \sum_{\mu=0}^{\mu_m} (2J^\mu + 1) \exp[-E^\mu/kT] + \int_{E^{\mu_m}}^{E^{m_{\text{ax}}}} \sum_{J^\mu, \pi^\mu} (2J^\mu + 1) \exp(-\epsilon/kT) \rho(\epsilon, J^\mu, \pi^\mu) d\epsilon, \quad (7)$$

where  $\rho(\epsilon, J^\mu, \pi^\mu)$  denotes the level density function and  $\mu_m$  is the label of the last employed either experimentally known or theoretically estimated energy state. The sum runs over all thermally discrete excited states up to  $\mu_m$ . In Eq. (7) the first term shows contribution from experimentally known low energy states as well as pn-QRPA calculated theoretical energy eigenvalues up to  $E^\mu$  while second term denotes contribution from remaining continuous states. The continuous excited states contribution was calculated using level density formula  $\rho(\epsilon, J^\mu, \pi^\mu)$ . We used the pn-QRPA model to calculate all discrete energy levels, up to 10 MeV, for all nuclide under consideration. Formalism for calculation of nuclear energy levels within the pn-QRPA formalism may be seen from (Muto et al. 1992; Nabi & Klapdor-Kleingrothaus 1999; Nabi & Klapdor-Kleingrothaus 2004) and is not reproduced here for space consideration. We incorporated the latest experimental data into our calculation for increased reliability, wherever possible. The calculated excitation energy was replaced with an experimental one when they were within 0.5 MeV of each other (missing measured states were inserted) along with their  $2J + 1$  values. For a particular nucleus, for measured (inserted) states with the missing angular momentum, the highest reported value of  $2J + 1$  was used. For cases where more than one value of  $J$  was reported, we selected the highest value.

Beyond 10 MeV energy scale and by assuming a uniform Fermi gas we estimated the level density (using saddle point approximation yields and some additional simplifications) as (Bohr & Mottelson 1969)

$$\rho(A, E) = \frac{\exp(2\sqrt{aE})}{4\sqrt{3E}}, \quad (8)$$

where  $a = \frac{\pi^2 g}{6}$  and the density of single particle states for a nucleus having  $A$  fermions is  $g = \frac{3A}{2\epsilon_f}$  and  $\epsilon_f$  is the

Fermi energy. Of course a more sophisticated treatment for calculation of the nuclear level density function is possible (e.g. back-shifted, pairing corrections, inclusion of spin cut-off parameters). It is to be noted that we microscopically calculated all energy levels up to 10 MeV in daughter. Beyond 10 MeV, the approximate formula used in Eq. (8) still gives us a reliable estimate of the level density for calculation of temperature-dependent nuclear partition functions to finally calculate the mass fractions in stellar matter (Eq. (1)).

The thermally distributed nuclei must conserve stellar mass

$$\sum_k X_k(A, Z) = 1. \quad (9)$$

Further conservation of charge demands

$$\sum_k \frac{X_k Z_k}{A_k} = \frac{(1 - \eta)}{2} = Y_e, \quad (10)$$

where  $Y_e$  depends on the electron number density given by  $n_e = N_0 \rho Y_e$ .

### 3 Results and Comparison

Fig. 1 depicts the nuclei present in our ensemble. There were a total of 728 *sd*-, *fp* and *fp**g*-shell nuclei present in our pool for calculation of mass fractions using the Saha Equation (Eq. (1)). The list of nuclei was inspired by the earlier calculation of weak-interaction rates in stellar matter by Nabi and Klapdor-Kleingrothaus (Nabi & Klapdor-Kleingrothaus 1999; Nabi & Klapdor-Kleingrothaus 2004).

The nuclear level density (NLD) is a key ingredient in the calculation of nuclear reaction rates in astrophysics. Typical outcomes of NLD calculation for nuclei in the Fe-region are shown in Fig. 2 and Fig.3. These seven nuclei are the same as the seven most abundant nuclei in NSE calculated by (Men-Quan et al. 2007) at  $T = 5 \times 10^9 \text{K}$  and  $\rho_{st} = 1 \times 10^{7-9} \text{g/cm}^3$ . It can be seen from the figures that  $^{58}\text{Ni}$  has the maximum level density and  $^{52}\text{Cr}$  the least which is also in agreement with the assumed level density function Eq. (8).

The temperature-dependent NPFs for few iron-regime nuclei as function of the stellar temperature  $T_9$  (which is measured in units of  $10^9 \text{K}$ ) are shown in Table 1. Our calculation is also compared with the statistical model calculation of (Rauscher & Thielemann 2000). The Hauser-Feshbach formalism was used by (Rauscher & Thielemann 2000) to perform a statistical model calculation of level densities and associated nuclear partition functions. The finite range droplet model (FRDM)

(Möller et al. 1995) was used as the input mass model to calculate the temperature-dependent NPFs by (Rauscher & Thielemann 2000). Whereas the two NPF calculations compare well for even-even nuclei, discrepancies of one order of magnitude or more are seen for odd-A and odd-odd cases. Authors in (Rauscher & Thielemann 2000) applied the statistical description throughout the nuclear chart without relying on experimental level density parameters in specific cases. The authors did comment that this feature of their formalism may lead to locally larger deviations from experiment. The microscopic calculation of theoretical energy levels (up to 10 MeV) and insertion of experimental energy levels resulted in a reliable and accurate estimate of NPF in our calculation. It is noted that the value of NPF increases as stellar temperature soars to high values. The rate of change of NPF increases with increasing temperatures. These effects may be traced down to Eq. (7).

We present our calculation of mass fractions in Fig. 4 and Fig. 5. The calculated mass fractions of eight most abundant nuclei at  $T = 5 \times 10^9 \text{K}$  and  $\rho_{st} = 1 \times 10^7 \text{g/cm}^3$  as a function of  $Y_e$  is shown in Fig. 4 and may be contrasted with Fig. 1 of (Men-Quan et al. 2007). It is seen from our Fig. 4 that the mass fractions increases monotonically with lepton content of the stellar matter. The difference with the calculation of (Men-Quan et al. 2007) is attributed to a more rigorous treatment of discrete energy levels up to 10 MeV for calculation of NPF, consideration of Coulomb correction in the binding energy of the nucleons and the choice of a much larger ensemble of nuclei in our mass fraction calculation. Fig. 5 depicts the evolution of mass fraction calculation of our eight most abundant nuclei at  $T = 5 \times 10^9 \text{K}$  and a higher stellar density of  $\rho_{st} = 1 \times 10^9 \text{g/cm}^3$  with increasing  $Y_e$ . Our Fig. 5 may be compared with Fig. 2 of (Men-Quan et al. 2007). It is noted in Fig. 5 that there is an inclusion of heavy nucleus,  $^{92}\text{Mo}$ , in the list of most abundant nuclei as stellar core stiffens to higher density. Moreover alphas are also very abundant at high stellar densities according to our calculation. A direct comparison of our calculation with those of (Men-Quan et al. 2007) can be seen in Table 2. The comparison of calculated mass fractions is shown at  $T = 5 \times 10^9 \text{K}$  and  $\rho_{st} = 1 \times 10^7 \text{g/cm}^3$  and  $Y_e = 0.5$ . It is evident from Table 2 that our model with new features leads to a much smaller calculated value of mass fractions (up to four orders of magnitude). In order to understand the origin of differences in the two calculations we lift some of the features of our calculation in order to come close to the conditions adopted by (Men-Quan et al. 2007) in their calculation of mass fraction. This new set of cal-

culcation can be seen in column 3 of Table 2. In order to perform our calculation with revised features we (i) summed the energy levels up to an excitation energy of 3 MeV, (ii) did not employ the Coulomb correction term in calculation of binding energies and (iii) chose a much smaller ensemble containing only iron-group nuclei in mass range 50 - 60. The smaller pool used for calculation of mass fractions containing only 89 nuclei can be seen in Fig. 6. We note that the two calculations still show differences. In order to further understand the origin of these differences we compare first the calculation of temperature-dependent NPFs used in the two mass fraction calculations for these six nuclei. Authors in (Men-Quan et al. 2007) used the calculated NPFs of (Rauscher & Thielemann 2000) till  $T_9 = 10$ . For still higher stellar temperatures they employed the NPF of (Rauscher 2003). We compare the temperature-dependent NPFs of the six nuclei with those of (Rauscher & Thielemann 2000) in Table 3 and with those of (Rauscher 2003) in Table 4. In addition to FRDM model, the extended Thomas-Fermi approach with Strutinski Integral (ETFISI) (Pearson et al. 1996) model was used by Rauscher as input mass formula for calculation of his NPFs at high temperatures. In Table 4 we compare our results with both mass models employed by Rauscher. Our calculated temperature-dependent NPFs are bigger up to an order of magnitude as compared to those by (Rauscher & Thielemann 2000) for odd-A nuclei. However we note that at higher temperatures, at times, the NPF calculated by (Rauscher 2003) is bigger by as much as an order of magnitude or more due to neglect of high temperature effects in our calculation. We further note that the calculated mass fractions depend heavily on the number of nuclei considered in the ensemble (see Eq. (9)). Whereas we took 89 nuclei in our smaller ensemble to compare our results with those of (Men-Quan et al. 2007), our calculated mass fractions could have increased by 1-3 orders of magnitude or more by choosing a much smaller ensemble (keeping other parameters of the calculation constant). It is to be noted that size of ensemble and its nuclear content were not mentioned by (Men-Quan et al. 2007). Lastly we attribute this difference to the microscopic calculation of energy levels (till an excitation energy of 3 MeV) in our model. We also incorporated measured energy levels in our calculation. For even-even nuclei the two models evidently calculate much different energy levels leading to the orders of magnitude differences. Our calculation with new features is in somewhat better agreement with that of (Men-Quan et al. 2007) for odd-A odd-Z nucleus  $^{55}\text{Co}$ . Within an isotopic chain, it is further noted that the two mass fraction calculations get in better agreement for heavier isotopes.

---

## 4 Conclusions

We presented here the mass fraction calculation in pre-supernova cores as a function of lepton content of the stellar matter. We assumed completion of silicon burning stage in our calculation which led us to exploit the conditions of NSE and use of Saha equation for the calculation of mass fractions. Our ensemble contained a total of 728 nuclei up to mass number 100. There are two distinguishing features of our mass fraction calculation. Firstly we included discrete energy levels (experimental and theoretical using the pn-QRPA model) up to 10 MeV excitation energy scale in the nucleus for the calculation of NPF. From 10-20 MeV we assumed a simple nuclear level density function and used method of integration to account for the continuum energy levels. Satisfactory convergence was achieved in our calculation of the NPF for presupernova conditions. Secondly we did not take the nucleus to be point-like and rather assumed spherical Wigner-Seitz cells for every nucleus. We then took into consideration the electron screening effect and inserted the Coulomb correction term in the binding energy of the nucleons. The resulting mass fractions were up to four orders of magnitude smaller than those calculated by (Men-Quan et al. 2007) and may significantly affect the rate of change of lepton-to-baryon ratio ( $\dot{Y}_e$ ) of stellar matter during presupernova evolution of massive stars. Fine-tuning of  $\dot{Y}_e$  is one of the keys to generate a successful explosion in core-collapse simulation. We are in a process of calculating  $\dot{Y}_e$  for typical presupernova conditions and hope to report this as a future assignment.

Whereas we presented the mass fractions for only the most abundant nuclei, the evolution of mass fractions with increasing  $Y_e$ , for all 728 nuclei under presupernova conditions, may be requested as ASCII files from the corresponding author. It is hoped that the mass fraction calculation presented here would prove useful for the analysis of stellar matter during presupernova phases of massive stars and for related network calculations.

**Acknowledgements** J.-U. Nabi wishes to acknowledge the support provided by the Higher Education Commission (Pakistan) through the HEC Project No. 20-3099. The work of A. Tawfik and N. Ezzelarab was supported by the World Laboratory for Cosmology and Particle Physics (WLCAPP).

## References

- Ptitsyn, D. A., and Chechetkin, V. M.: On nucleosynthesis in supernovae beyond the iron peak. *Soviet Astronomy Letters*, 8, 322 (1982).
- Woosley, S. E., and Hoffman, R. D.: The alpha-process and the r-process. *Astrophys. J.* 395, 202 (1992).
- Nadyozhin, D. K., Panov., I. V., and Blinnikov, S. I.: The neutrino-induced neutron source in helium shell and r-process nucleosynthesis. *Astron. Astrophys.* 335, 207 (1998).
- Hartmann, D., Woosley, S. E., and El Eid, M. F.: Nucleosynthesis in neutron-rich supernova ejecta. *Astrophys. J.* 297, 837 (1985).
- Hoyle, F.: On Nuclear Reactions Occuring in Very Hot STARS. I. the Synthesis of Elements from Carbon to Nickel. *Astrophys. J. Suppl. Ser.* 1, 121 (1954).
- Men-Quan, L., Jie, Z., and Zhi-Quan, L.: Nuclear statistical equilibrium at core-collapse supernova. *Chinese. Phys.* 16, 3146 (2007).
- Clifford, F. E., and Tayler, R. J.: The equilibrium distribution of nuclides in matter at high temperatures. *Mon. Not. R. Astron. Soc.* 129, 104 (1965).
- Epstein, R. I., and Arnett, W. D.: Neutronization and thermal disintegration of dense stellar matter. *Astrophys. J.* 201, 202 (1975).
- Aufderheide, M. B., Fushiki, I., Woosley, S. E., and Hartmann, D. H.: Search for important weak interaction nuclei in presupernova evolution. *Astrophys. J. Suppl. Ser.* 91, 389 (1994).
- Bravo, E., and García-Senz, D.: Coulomb corrections to the equation of state of nuclear statistical equilibrium matter: implications for SNIa nucleosynthesis and the accretion-induced collapse of white dwarfs. *Mon. Not. R. Astron. Soc.* 307, 984 (1999).
- Fischer, T., Hempel, M., Sagert, I., Suwa, Y., and Schaffner-Bielich, J.: Symmetry energy impact in simulations of core-collapse supernovae. *Eur. Phys. J. A.* 50, 1 (2014).
- Nabi J. -U., Tawfik, A. N., Ezzelarab, N., and Khan, A. A.: Nuclear level densities, partition functions and abundances in stellar interior *Phy. Scr.* (submitted) (2015).
- Fuller, G. M.: Neutron shell blocking of electron capture during gravitational collapse. *Astrophys. J.* 252, 741 (1982).
- Hix, W. R., and Thielemann F. -K.: Silicon Burning. I.: Neutronization and the Physics of Quasi-Equilibrium. *Astrophys. J.* 460, 869 (1996).
- Dimarco, A., Barbero, C., Dias, H., Garcia, F., Horvath, J., and Losano, L.: Influence of low-lying discrete nuclear states on isotopic abundances in presupernova cores. *J. Phys. G.* 28, 121 (2002).
- Kodama, T., and Takahashi, K.: R-process nucleosynthesis and nuclei far from the region of  $\beta$ -stability. *Nucl. Phys. A.* 239, 489 (1975).
- Chamel, N., Naimi, S., Khan, E., and Margueron, J.: Validity of the Wigner-Seitz approximation in neutron star crust. *Phys. Rev. C* 75, 055806 (2007).
- Fowler, W. A., Caughlan, G. R., and Zimmerman, B. A.: Thermonuclear reaction rates. *Ann. Rev. Astr. Astrophys.* 5, 525 (1967).
- Muto, K. A. Z. U. O., Bender, E., Oda, T., and Klapdor-Kleingrothaus, H. V.: Proton-neutron quasiparticle RPA with separable Gamow-Teller forces. *Zeit. Phys. A.* 341(4), 407 (1992).
- Nabi, J. -U., and Klapdor-Kleingrothaus, H. V.: Microscopic calculations of weak interaction rates of nuclei in stellar environment for  $A=18$  to 100. *Eur. Phys. J. A.* 5, 337 (1999).
- Nabi, J. -U., and Klapdor-Kleingrothaus, H. V.: Microscopic calculations of stellar weak interaction rates and energy losses for fp-and fp<sub>g</sub>-shell nuclei. *At. Data Nucl. Data Tables.* 88, 237 (2004).
- Bohr, A., and Mottelson, B. R.: *Nuclear Structure (Vol. 1)* (Benjamin, New York 1969).
- Rauscher, T., and Thielemann, F.-K.: Astrophysical reaction rates from statistical model calculations. *At. Data Nucl. Data Tables.* 75, 1 (2000).
- Möller, P., Nix, J. R., Myers, W. D., and Swiatecki, W.J.: Nuclear ground-state masses and deformations. *At. Data Nucl. Data Tables.* 59, 185 (1995).
- Rauscher, T.: Nuclear Partition Functions at Temperatures Exceeding  $10^{10}$ K. *Astrophys. J. Suppl. Ser.* 147, 403 (2003).
- Pearson, J. M., Nayak, R. C., and Goriely S.: Nuclear mass formula with Bogolyubov-enhanced shell-quenching: application to r-process. *Phys. Lett. B* 387, 455 (1996).

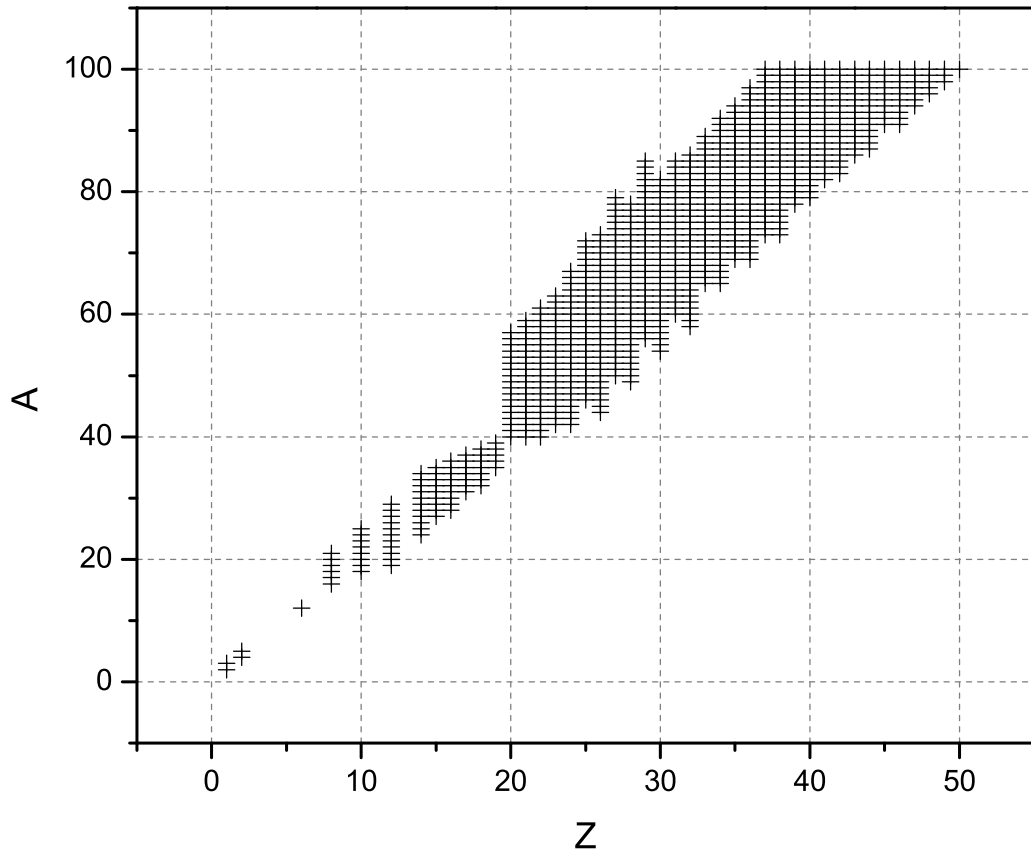


**Fig. 1** Nuclei present in our ensemble for mass fraction calculation.

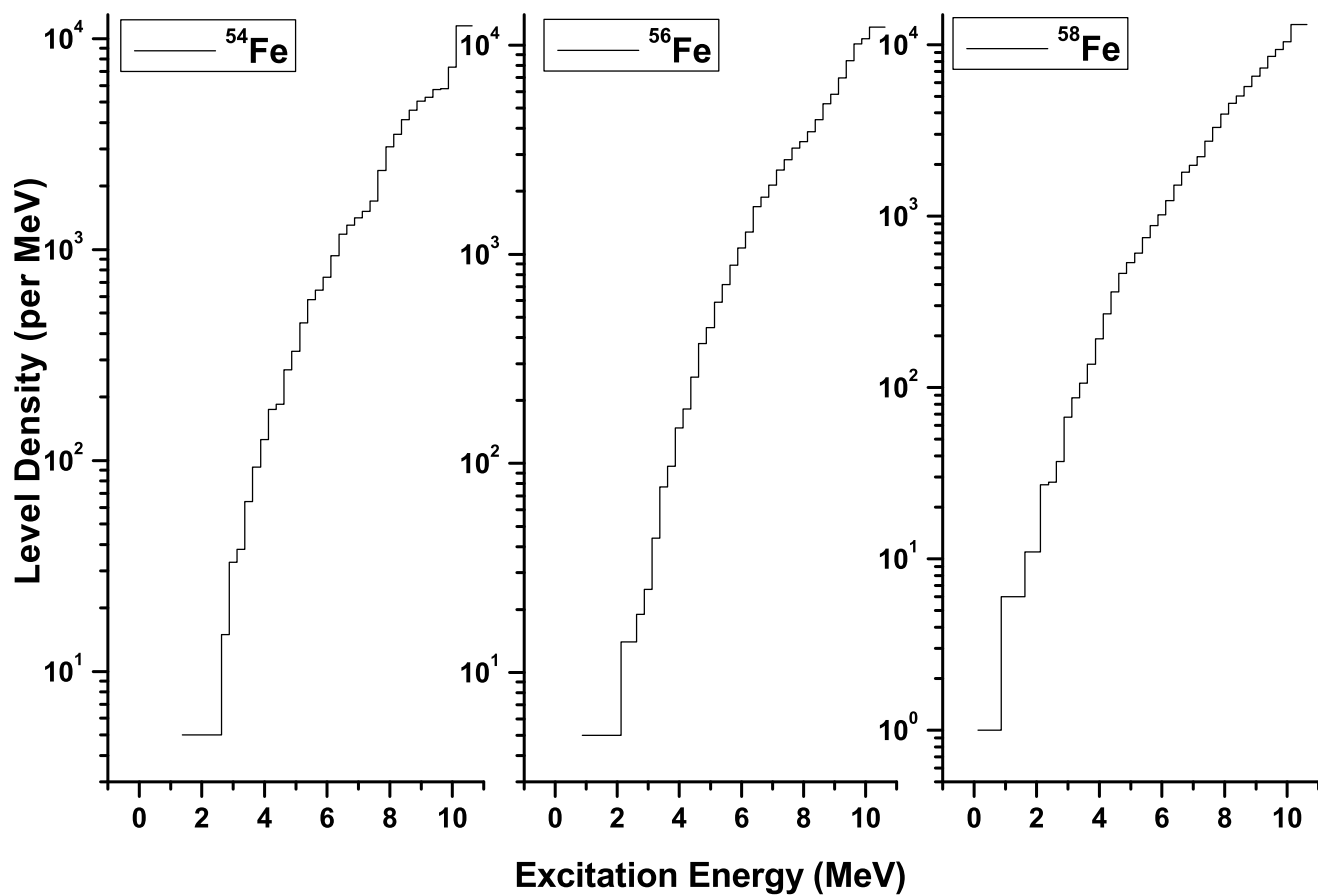
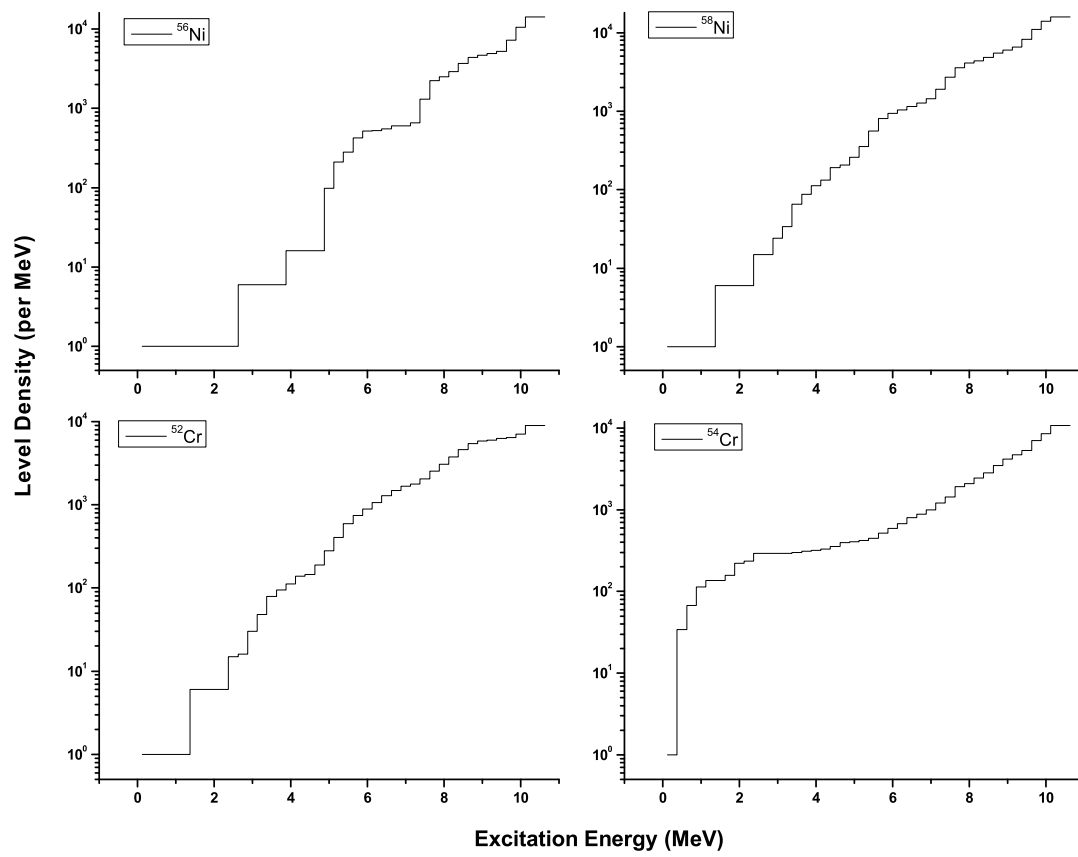
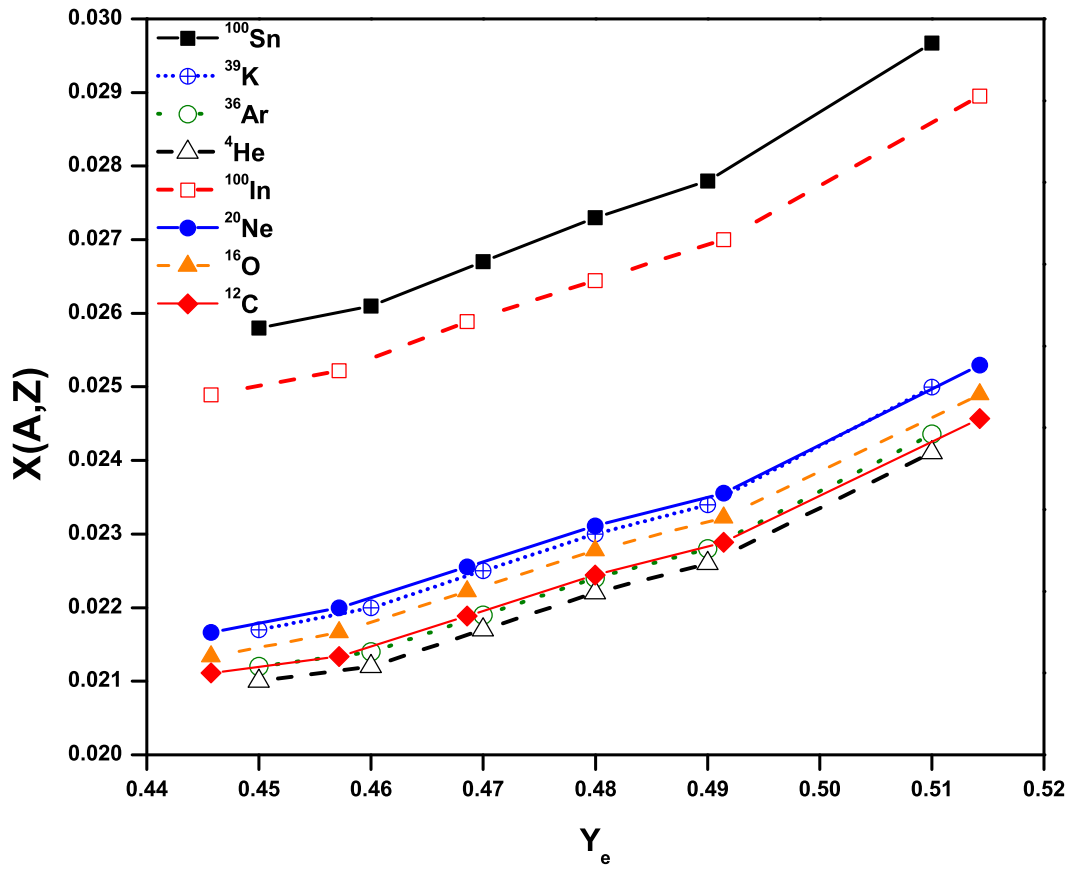


Fig. 2 Calculated nuclear level densities for iron isotopes.



**Fig. 3** Calculated nuclear level densities for Fe-region nuclei.



**Fig. 4** Mass fractions of the eight most abundant nuclei as function of  $Y_e$  at  $T = 5 \times 10^9 \text{K}$  and  $\rho_{st} = 1 \times 10^7 \text{g/cm}^3$  (color online).

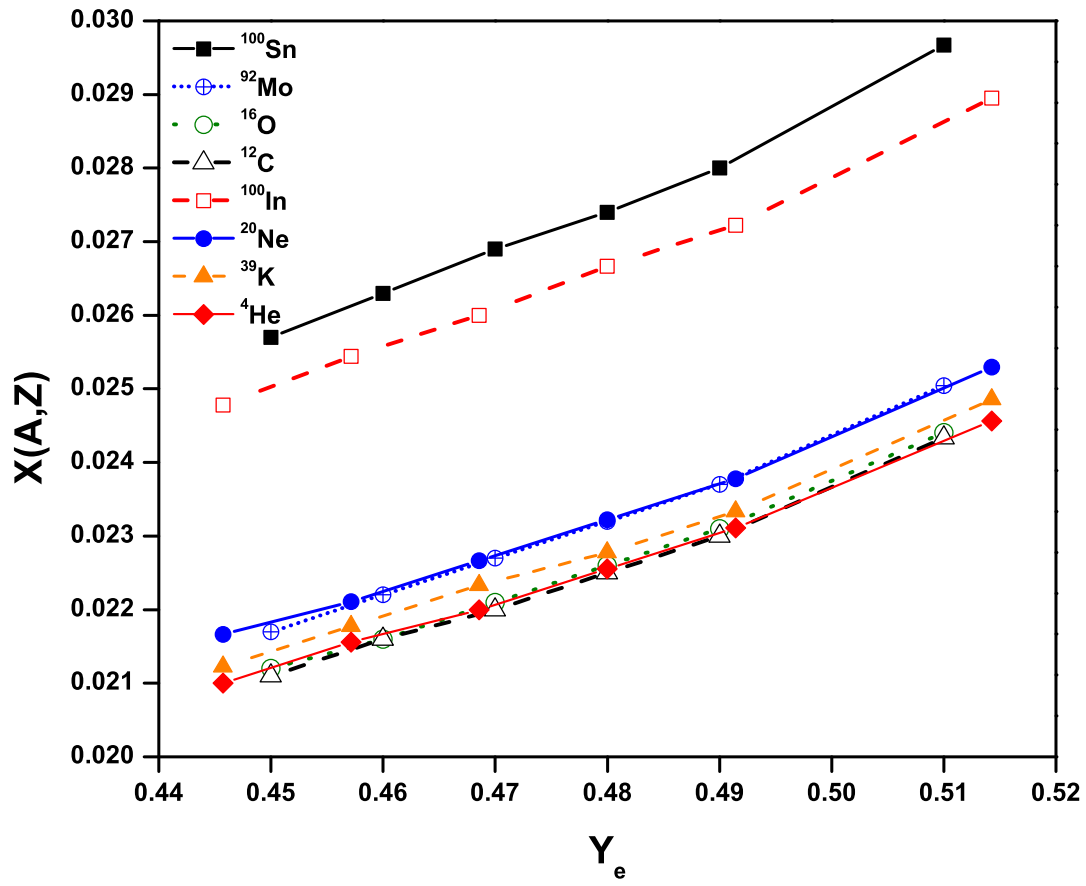


**Fig. 5** Mass fractions of the eight most abundant nuclei as function of  $Y_e$  at  $T = 5 \times 10^9 \text{K}$  and  $\rho_{st} = 1 \times 10^9 \text{g/cm}^3$  (color online).

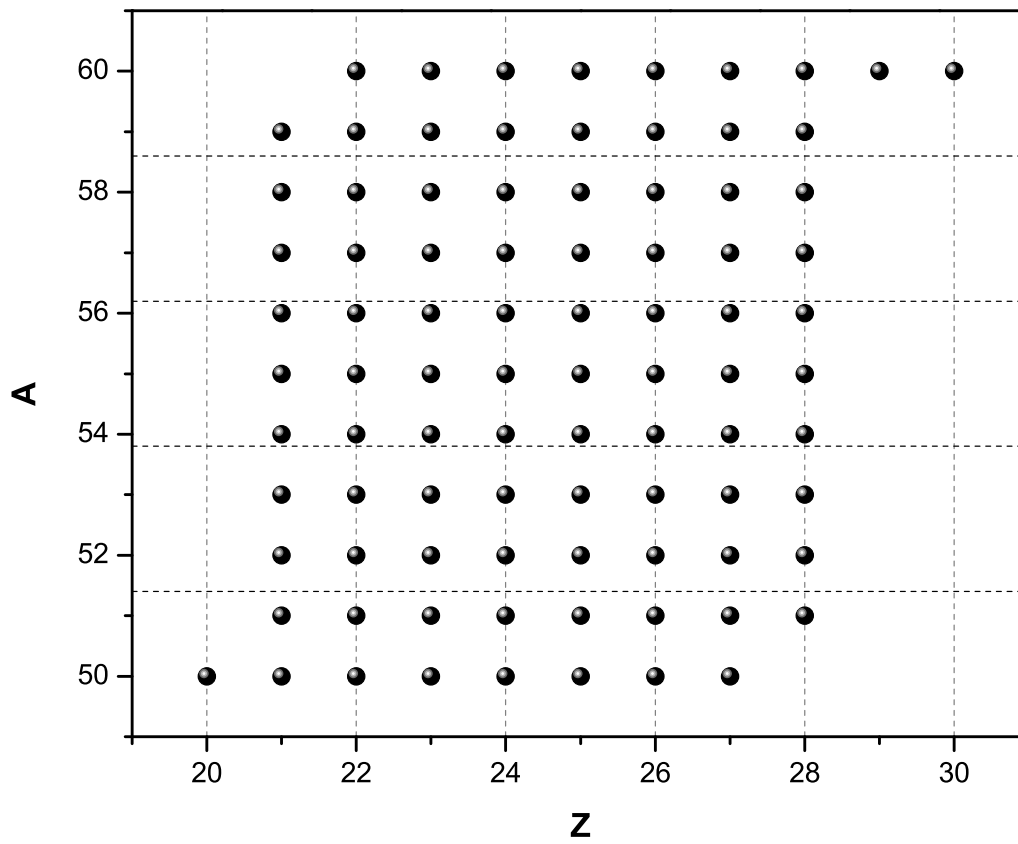


**Fig. 6** Nuclei present in our smaller ensemble for mass fraction calculation with revised features.

**Table 1** Calculated temperature dependent nuclear partition functions for  $^{50,51}\text{Sc}$ ,  $^{50,51}\text{Ti}$ ,  $^{50,51}\text{V}$ ,  $^{50,51}\text{Cr}$ ,  $^{50,51}\text{Mn}$ ,  $^{50,51}\text{Fe}$ ,  $^{50,51}\text{Co}$  and  $^{51,52}\text{Ni}$  compared with the earlier statistical calculation of (Rauscher & Thielemann 2000) denoted by RT. Numbers in parenthesis indicate stellar temperature in units of  $10^9\text{K}$ .

Nuclei	This work		RT		This work		RT	
	G (1.0)	G (2.0)	G (1.0)	G (2.0)	G (3.0)	G (5.0)	G (10.0)	G (30.0)
$^{50}\text{Sc}$	1.219E+01	1.037E+00	1.818E+01	1.391E+00	5.307E+01	4.1E+00		
	1.499E+01	1.207E+00	2.452E+01	1.723E+00	1.456E+05	.....		
$^{51}\text{Sc}$	1.153E+01	1.000E+00	1.665E+01	1.057E+00	3.447E+01	5.1E+00		
	1.470E+01	1.008E+00	1.999E+01	1.373E+00	3.170E+03	.....		
$^{50}\text{Ti}$	1.000E+00	1.000E+00	1.000E+00	1.013E+00	2.503E+00	3.8E+00		
	1.000E+00	1.001E+00	1.006E+00	1.165E+00	3.365E+03	.....		
$^{51}\text{Ti}$	4.840E+00	1.000E+00	5.510E+00	1.018E+00	2.214E+01	4.1E+00		
	5.113E+00	1.001E+00	6.898E+00	1.197E+00	3.224E+04	.....		
$^{50}\text{V}$	2.972E+00	1.091E+00	1.531E+01	1.876E+00	1.106E+02	6.9E+00		
	8.773E+00	1.461E+00	3.139E+01	2.745E+00	1.345E+05	.....		
$^{51}\text{V}$	9.025E+00	1.018E+00	1.320E+01	1.235E+00	4.156E+01	3.4E+00		
	1.092E+01	1.120E+00	1.830E+01	1.488E+00	3.108E+04	.....		
$^{50}\text{Cr}$	1.000E+00	1.001E+00	1.248E+00	1.248E+00	6.918E+00	7.6E+00		
	1.053E+00	1.053E+00	1.956E+00	1.964E+00	3.139E+03	.....		
$^{51}\text{Cr}$	1.379E+00	1.000E+00	1.948E+00	1.067E+00	8.825E+00	4.4E+00		
	1.692E+00	1.011E+00	2.434E+00	1.381E+00	2.918E+04	.....		
$^{50}\text{Mn}$	3.107E+00	1.048E+00	1.062E+01	6.825E+00	6.270E+01	4.3E+01		
	6.671E+00	4.233E+00	2.002E+01	1.223E+01	1.215E+05	.....		
$^{51}\text{Mn}$	2.055E+00	1.085E+00	5.324E+00	1.562E+00	2.897E+01	5.1E+00		
	3.806E+00	1.339E+00	8.501E+00	2.015E+00	2.999E+04	.....		
$^{50}\text{Fe}$	1.001E+00	1.000E+00	1.266E+00	1.025E+00	6.249E+00	8.3E+00		
	1.059E+00	1.002E+00	1.989E+00	1.336E+00	3.125E+03	.....		
$^{51}\text{Fe}$	7.364E+00	1.064E+00	1.037E+01	1.511E+00	3.041E+01	4.1E+00		
	8.863E+00	1.296E+00	1.383E+01	1.890E+00	2.993E+04	.....		
$^{50}\text{Co}$	1.359E+01	1.048E+00	1.545E+01	1.281E+00	3.446E+01	5.9E+00		
	1.451E+01	1.147E+00	1.755E+01	1.718E+00	1.334E+05	.....		
$^{51}\text{Co}$	8.233E+00	1.000E+00	8.831E+00	1.020E+00	1.558E+01	2.4E+00		
	8.556E+00	1.003E+00	9.317E+00	1.117E+00	2.909E+04	.....		
$^{51}\text{Ni}$	8.836E+00	1.085E+00	9.762E+00	1.462E+00	1.520E+01	8.0E+00		
	9.405E+00	1.250E+00	1.026E+01	2.095E+00	3.107E+04	.....		
$^{52}\text{Ni}$	1.000E+00	1.000E+00	1.000E+00	1.001E+00	2.656E+00	3.3E+00		
	1.000E+00	1.000E+00	1.013E+00	1.032E+00	3.671E+03	.....		

**Table 2** Calculated mass fractions for  $^{52,53,54}\text{Fe}$ ,  $^{55}\text{Co}$  and  $^{56,58}\text{Ni}$  at temperature  $T = 5 \times 10^9 \text{K}$ ,  $\rho_{st} = 1 \times 10^7 \text{g.cm}^{-3}$  and  $Y_e = 0.5$  compared with the calculation of (Men-Quan et al. 2007).

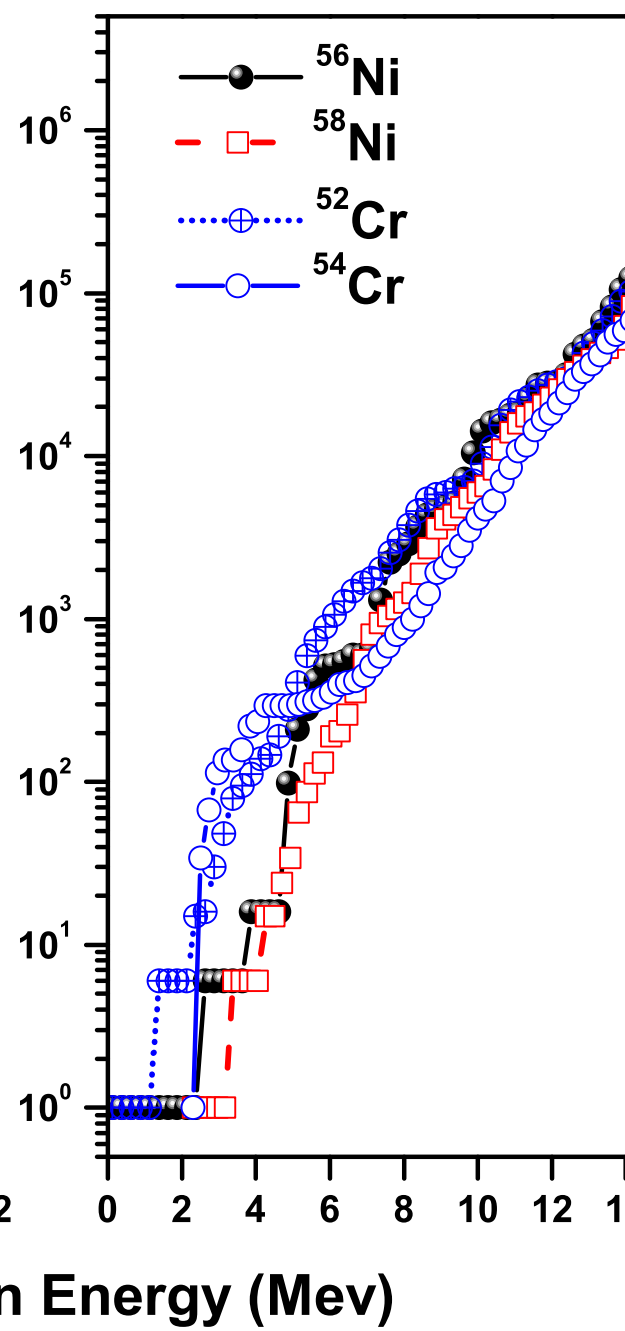
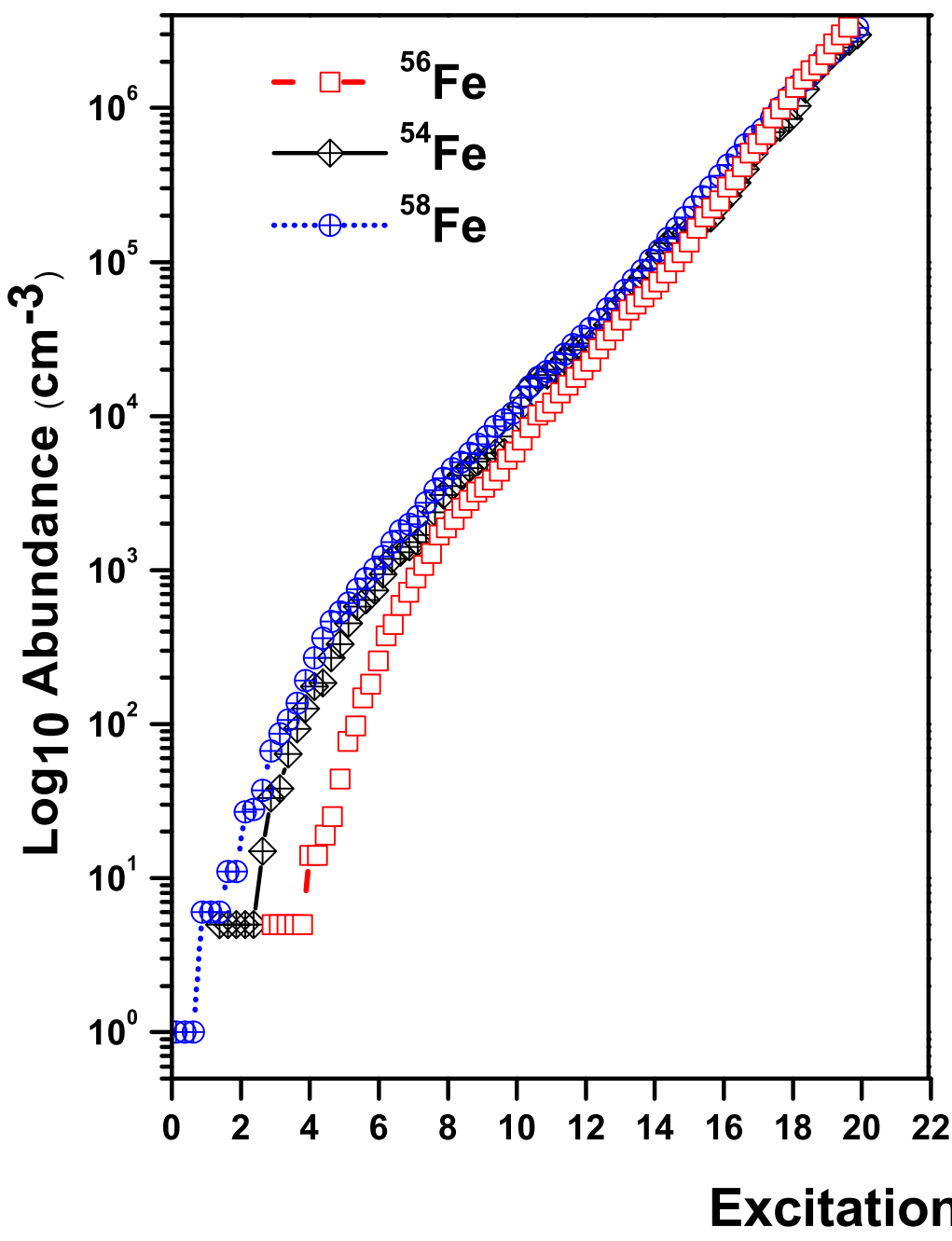
Nuclei	$X(A, Z)$ (this work with new features)	$X(A, Z)$ (this work with revised features)	$X(A, Z)$ (Men-Quan et al. 2007)
$^{52}\text{Fe}$	$1.573 \times 10^{-6}$	$5.901 \times 10^{-6}$	$2.581 \times 10^{-2}$
$^{53}\text{Fe}$	$3.629 \times 10^{-5}$	$1.361 \times 10^{-4}$	$3.653 \times 10^{-2}$
$^{54}\text{Fe}$	$6.792 \times 10^{-3}$	$2.547 \times 10^{-2}$	$2.984 \times 10^{-1}$
$^{55}\text{Co}$	$1.085 \times 10^{-3}$	$2.689 \times 10^{-2}$	$2.868 \times 10^{-2}$
$^{56}\text{Ni}$	$4.545 \times 10^{-5}$	$1.705 \times 10^{-4}$	$3.978 \times 10^{-1}$
$^{58}\text{Ni}$	$8.769 \times 10^{-3}$	$3.288 \times 10^{-2}$	$1.065 \times 10^{-1}$

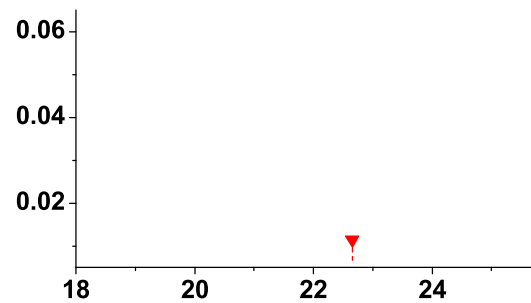
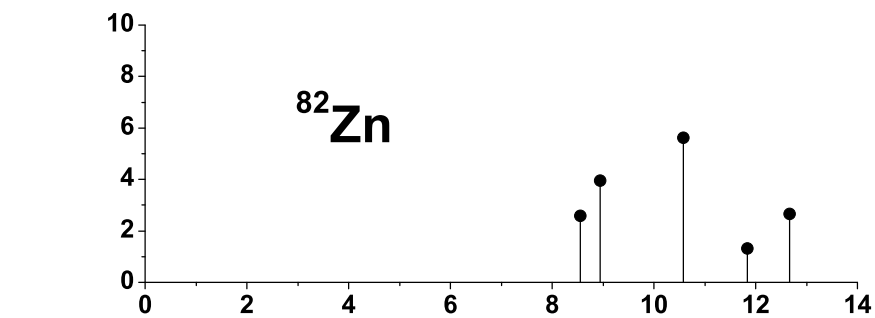
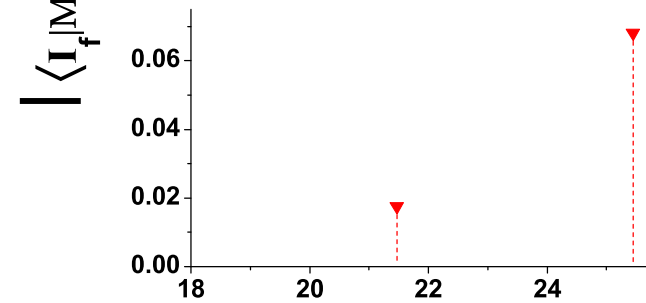
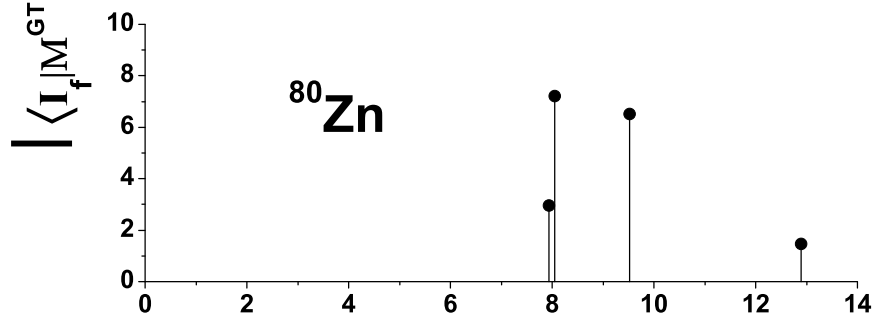
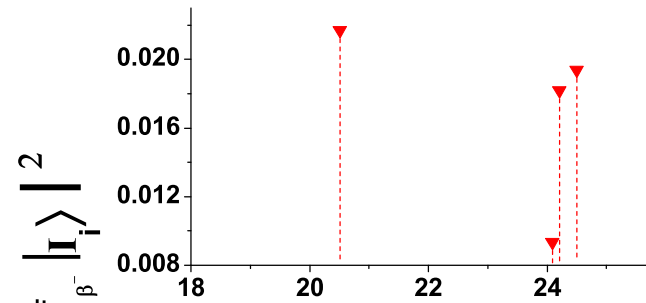
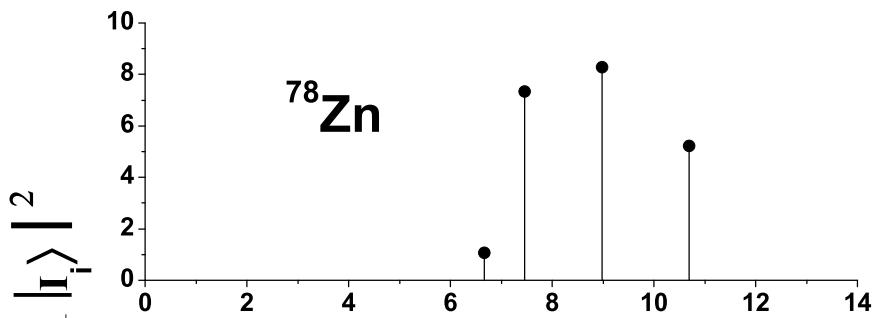
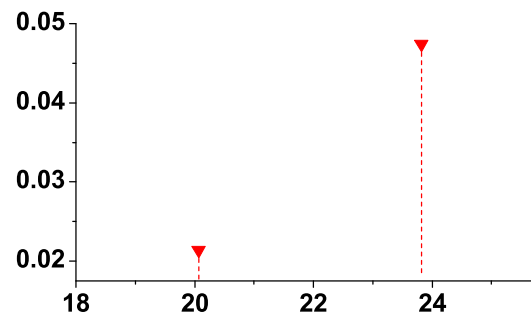
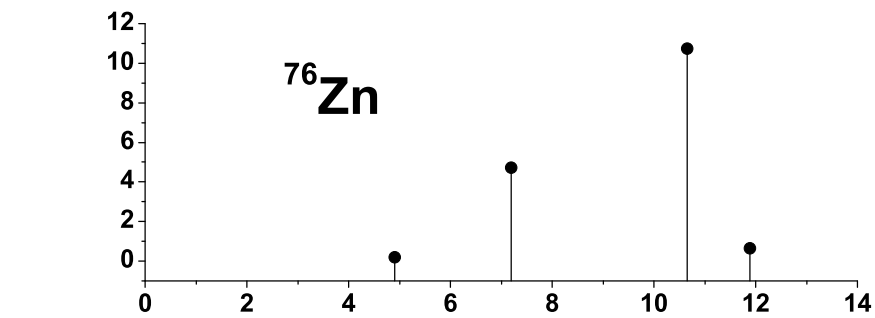
**Table 3** Comparison of calculated temperature-dependent partition functions ( $G$ ) with those of (Rauscher & Thielemann 2000) for  $^{52,53,54}\text{Fe}$ ,  $^{55}\text{Co}$  and  $^{56,57,58}\text{Ni}$ . Numbers in parenthesis give stellar temperature in units of  $10^9 \text{K}$ .

Nuclei	$G(0.01,0.5,1)$	$G(0.01,0.5,1)$	$G(2,4,5)$	$G(2,4,5)$	$G(6,8,10)$	$G(6,8,10)$
	QRPA	FRDM	QRPA	FRDM	QRPA	FRDM
$^{52}\text{Fe}$	1.00E+00	1.00E+00	1.04E+00	1.04E+00	2.14E+00	2.10E+00
	1.00E+00	1.00E+00	1.44E+00	1.44E+00	3.38E+00	3.00E+00
	1.00E+00	1.00E+00	1.75E+00	1.74E+00	6.01E+00	4.57E+00
$^{53}\text{Fe}$	8.00E+00	1.00E+00	8.74E+00	1.01E+00	1.37E+01	1.46E+00
	8.10E+00	1.00E+00	1.03E+01	1.14E+00	2.01E+01	2.13E+00
	8.33E+00	1.00E+00	1.16E+01	1.27E+00	3.24E+01	3.58E+00
$^{54}\text{Fe}$	1.00E+00	1.00E+00	1.00E+00	1.00E+00	1.60E+00	1.55E+00
	1.00E+00	1.00E+00	1.10E+00	1.10E+00	3.18E+00	2.75E+00
	1.00E+00	1.00E+00	1.27E+00	1.26E+00	7.04E+00	5.54E+00
$^{55}\text{Co}$	8.00E+00	1.00E+00	8.73E+00	1.00E+00	1.03E+01	1.05E+00
	8.05E+00	1.00E+00	9.43E+00	1.00E+00	1.30E+01	1.26E+00
	8.26E+00	1.00E+00	9.78E+00	1.01E+00	2.12E+01	1.96E+00
$^{56}\text{Ni}$	1.00E+00	1.00E+00	1.00E+00	1.00E+00	1.05E+00	1.03E+00
	1.00E+00	1.00E+00	1.00E+00	1.00E+00	1.41E+00	1.18E+00
	1.00E+00	1.00E+00	1.01E+00	1.01E+00	2.97E+00	1.67E+00
$^{58}\text{Ni}$	1.00E+00	1.00E+00	1.00E+00	1.00E+00	1.57E+00	1.51E+00
	1.00E+00	1.00E+00	1.09E+00	1.09E+00	3.14E+00	2.71E+00
	1.00E+00	1.00E+00	1.25E+00	1.24E+00	7.28E+00	5.75E+00

**Table 4** Comparison of calculated temperature-dependent partition functions ( $G$ ) with those of (Rauscher 2003) for  $^{52,53,54}\text{Fe}$ ,  $^{55}\text{Co}$  and  $^{56,57,58}\text{Ni}$ . Numbers in parenthesis give stellar temperature in units of  $10^9 \text{K}$ .

Nuclei	$G(12,14,16)$	$G(12,14,16)$	$G(12,14,16)$	$G(18,20,22)$	$G(18,20,22)$	$G(18,20,22)$	$G(24,26,28)$	$G(24,26,28)$	$G(24,26,28)$
	QRPA	ETFSI	FRDM	QRPA	ETFSI	FRDM	QRPA	ETFSI	FRDM
$^{52}\text{Fe}$	1.19E+01	7.72E+00	8.23E+00	1.13E+02	1.11E+02	1.39E+02	8.03E+02	2.29E+03	3.19E+03
	2.49E+01	1.64E+01	1.86E+01	2.30E+02	3.05E+02	3.99E+02	1.37E+03	6.15E+03	8.84E+03
	5.32E+01	4.09E+01	4.91E+01	4.43E+02	8.40E+02	1.14E+03	2.21E+03	1.63E+04	2.42E+04
$^{53}\text{Fe}$	5.87E+01	7.07E+00	6.88E+00	7.21E+02	8.28E+01	8.22E+01	6.80E+03	1.23E+03	1.31E+03
	1.24E+02	1.52E+01	1.48E+01	1.67E+03	2.01E+02	2.04E+02	1.22E+04	3.06E+03	3.37E+03
	2.97E+02	3.48E+01	3.40E+01	3.51E+03	4.96E+02	5.14E+02	2.03E+04	7.63E+03	8.72E+03
$^{54}\text{Fe}$	1.54E+01	1.25E+01	1.23E+01	1.36E+02	2.11E+02	2.09E+02	9.07E+02	4.23E+03	4.47E+03
	3.24E+01	3.04E+01	2.97E+01	2.69E+02	5.72E+02	5.76E+02	1.53E+03	1.14E+04	1.24E+04
	6.71E+01	7.86E+01	7.70E+01	5.08E+02	1.56E+03	1.60E+03	2.46E+03	3.08E+04	3.46E+04
$^{55}\text{Co}$	4.48E+01	4.02E+00	3.86E+00	7.66E+02	5.62E+01	5.45E+01	7.49E+03	9.39E+02	9.80E+02
	1.13E+02	9.23E+00	8.81E+00	1.80E+03	1.42E+02	1.41E+02	1.34E+04	2.44E+03	2.63E+03
	2.99E+02	2.25E+01	2.15E+01	3.85E+03	3.64E+02	3.69E+02	2.24E+04	6.35E+03	7.11E+03
$^{56}\text{Ni}$	7.81E+00	3.20E+00	3.23E+00	1.19E+02	6.76E+01	7.17E+01	9.74E+02	1.74E+03	2.01E+03
	2.06E+01	8.03E+00	8.19E+00	2.59E+02	2.01E+02	2.19E+02	1.70E+03	5.10E+03	6.08E+03
	5.12E+01	2.28E+01	2.37E+01	5.21E+02	5.94E+02	6.64E+02	2.79E+03	1.48E+04	1.83E+04
$^{58}\text{Ni}$	1.67E+01	1.38E+01	1.38E+01	1.64E+02	2.98E+02	3.10E+02	1.15E+03	7.47E+03	8.42E+03
	3.69E+01	3.66E+01	3.69E+01	3.30E+02	8.72E+02	9.29E+02	1.96E+03	2.18E+04	2.54E+04
	7.89E+01	1.03E+02	1.05E+02	6.33E+02	2.55E+03	2.80E+03	3.16E+03	6.35E+04	7.67E+04





Daughter Energy (MeV)